analytical chemistry

pubs.acs.org/ac Article

A Dual-Mode Fluorescent Nanoprobe for the Detection and Visual Screening of Pathogenic Bacterial Spores

Xiwen Ye, Jingkang Li, Dejiang Gao, Pinyi Ma,* Qiong Wu,* and Daqian Song*

Cite This: *Anal. Chem.* 2024, 96, 6012−6020 Read Online

ACCESS | Metrics & More | Article Recommendations | Supporting Information

ABSTRACT: Bacterial vegetative cells turn into metabolically dormant spores in certain environmental situations. Once suitable conditions trigger the germination of spores belonging to the pathogenic bacterial category, public safety and environmental hygiene will be threatened, and lives will even be endangered when encountering fatal ones. Instant identification of pathogenic bacterial spores remains a challenging task, since most current approaches belonging to complicated biological methods unsuitable for onsite sensing or emerging alternative chemical techniques are still inseparable from professional instruments. Here we developed a polychromatic fluorescent nanoprobe for ratiometric detection and visual inspection of the pathogenic bacterial spore biomarker, dipicolinic acid (DPA), realizing rapidly accurate screening of pathogenic bacterial spores such as *Bacillus anthracis* spores. The nanoprobe is made of aminoclay-coated silicon nanoparticles and functionalized with europium ions, exhibiting selective and sensitive response toward DPA and *Bacillus subtilis* spores (simulants for *Bacillus anthracis* spores) with excellent linearity. The proposed sensing strategy allowing spore determination of as few as 0.3×10^5 CFU/mL within 10 s was further applied to real environmental sample detection with good accuracy and reliability. Visual quantitative determination can be achieved by analyzing the RGB values of the corresponding test solution color via a color recognition APP on a smartphone. Different test samples can be photographed at the same time, hence the efficient accomplishment of examining bulk samples within minutes. Potentially employed in various on-site sensing occasions, this strategy may develop into a powerful means for distinguishing hazardous pathogens to facilitate timely and proper actions of dealing with multifarious security issues.

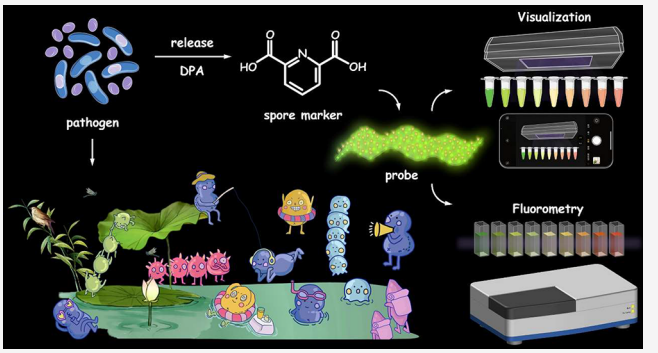

INTRODUCTION

Bacterial spores generated in the process of sporulation by bacteria cells[1] possess the most resistant microbial structures toward a variety of severe environments and bactericidal stress,[2] such as heat, freezing, desiccation, ultraviolet radiation, high pressure, extreme pH, chemicals.[3,4] Even when the bacteria organisms are killed, the spores can still survive and remain viable in their dormant resistant state for decades or yet thousands of years in adverse environmental conditions.[5,6] Once the surrounding conditions are conducive to growth, the spores will break dormancy and transform into vegetatively growing cells in the process of germination followed by outgrowth, giving rise to spoilage or producing toxins.[1] Especially, pathogenic bacterial spores always readily cause food poisoning, health issues, and environment problems,[7,8] while the more lethal ones even pose great threats to public safety and homeland security as fatal biological warfare agents and bioterrorism weapons.[9,10] Among the potential bioweapon candidates, *Bacillus anthracis* spores (*B. anthracis* spores) are of particular concern as the anthrax attacks of 2001.[11,12] Anthracis spores when dispersed through aerosol extensively contaminate air, water, and food in large areas simultaneously,[13] ascribable to their relatively simple production process into weapon-grade stuff outside laboratories.[14] Inhalation of over 10^4 *B. anthracis* spores is deadly unless there is medical treatment within 24−48 h; hence, they are extremely hazardous for human beings who can be infected with anthrax through direct or indirect contact with the bacteria spores.[15,16] Accordingly, sensitively accurate sensing of pathogenic bacterial spores is vital for early warning of associated security incidents.

As for *B. anthracis* spores, microscopic staining techniques[17] and polymerase chain reaction (PCR)[18] are standard biological means of diagnosing suspected specimens whether with anthrax infections or not, and immunoassays also count as another important diagnostic method.[19] However, staining

Received: January 23, 2024
Revised: March 18, 2024
Accepted: March 22, 2024
Published: April 2, 2024

https://doi.org/10.1021/acs.analchem.4c00443
Anal. Chem. 2024, 96, 6012−6020

Scheme 1. Fabrication Process of the Probe and the Sensing Mechanism of the Proposed Strategy: (A) Synthesis of the Precursor SiNPs, (B) Preparation of the Probe, and (C) Sensing Process of the Probe

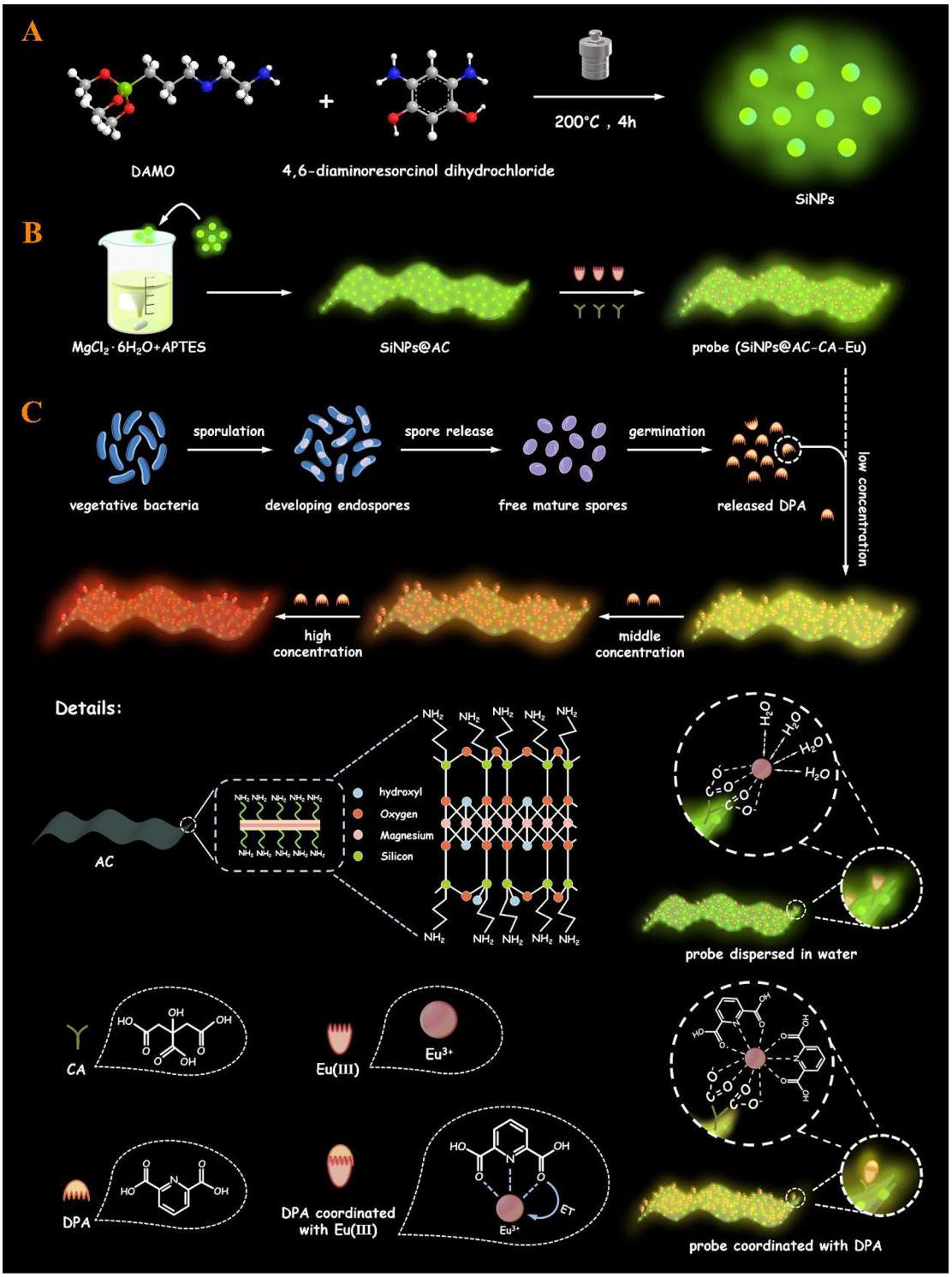

microscopic specimens contains assorted time-consuming procedures except for the need of microscopic apparatus and selection of appropriate staining protocol.[17] PCR as a primer-mediated enzymatic DNA amplification method requires expensive reagents and considerable sample pretreatment prior to analysis,[20] while immunoassays based on interaction between antibodies and cell surface antigens demand the utilization of specific antibodies for desired agents and respective adjustment of mobile-phase conditions for their capture, elution, and separation.[14] In consequence, even if the causative organism is confirmed by these methods, it is very likely to miss the golden time for medical treatments since the bacterial infections might have induced severe anatomical damages, even lethal hazards.[21] 2,6-Dipicolinic acid (also known as dipicolinic acid, DPA), demonstrated as a significant biomarker of most pathogenic bacteria spores[22] distinguished

https://doi.org/10.1021/acs.analchem.4c00443
Anal. Chem. 2024, 96, 6012−6020

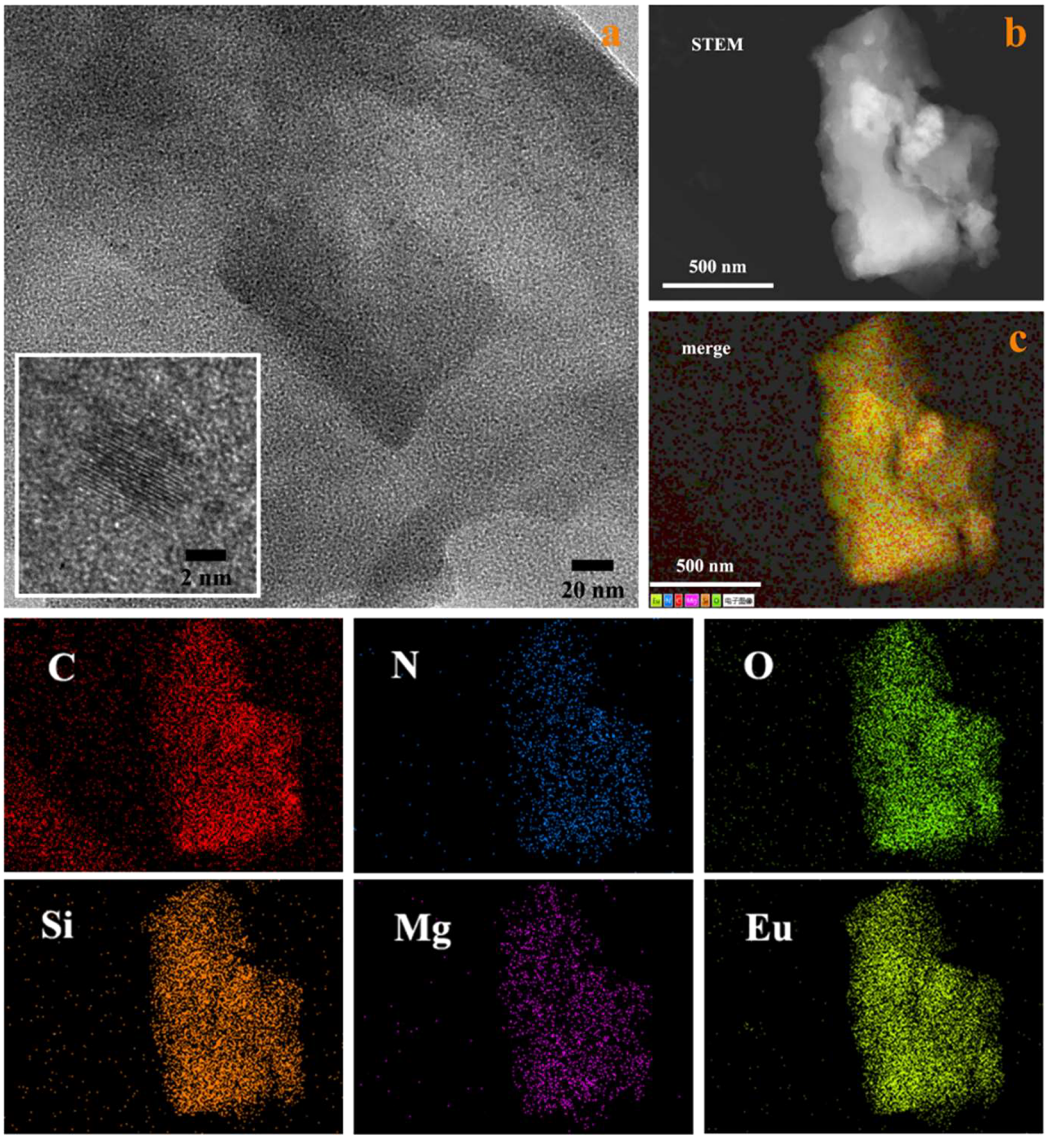

Figure 1. (a) TEM image of the probe. Inset is the high-resolution TEM image of the SiNPs loaded on the probe. (b) HAADF-STEM micrograph of the probe. (c) The rest of the images are the EDS elemental mapping results of the probe.

from other common spores like pollen or mold, is an essential component of spores.[17] Large amounts of DPA exists in such protective layers that surround the innermost core of spores, accounting for 5−15% of the dry mass.[23] When suffered from physical lysis, either chemical lysis or triggered for germination, dipicolinic acid will be released.[24,25] Among numerous approaches relying on testing of DPA, fluorescence spectrometry shows valuable merits of simplicity, rapidity, high sensitivity, excellent selectivity, high throughput, and visible observation,[26,27] which appears more suitable for rapid or on-site detection.

As previously reported, lanthanide ions are endowed with unique optical and spectral properties such as long fluorescent lifetime, intrinsic narrow f−f emission bands, and large Stokes shifts.[28,29] Consequently, lanthanide-based probes for detection of DPA have evolved, most of which were according to single-emission mechanism of either fluorescence turning on mode or turning off mode.[30−33] However, the brightness change of single color may suffer from disturbances of surroundings or instrumental factors and constrain the visual determination potential. Of note, ratiometric fluorometry occupies unique status with self-calibration capability and resists plenty of analyte-independent factors,[34,35] thence owning reliability and reproducibility and improving precision and sensitivity of the analytical performance, superior to single-emission fluorometry.[36] Silicon nanoparticles (SiNPs), as a newly rising nanomaterial featuring strong fluorescence accompanied by robust photostability and benign biocompatibility coupled with favorable biodegradability,[37] are competitive candidates for construction of fluorescent sensors.[38] Furthermore, aminoclay (AC), a synthetic organic layered clay containing abundant amino functional groups with a talc-like structure,[39] can serve as an attractive substrate for nanoparticles to prepare multifunctional hybrid nanomaterials, since the amino group as a strong nucleophile provides extensive potential in covalent modification of AC via amidation reaction, nucleophilic substitution, Michael-like addition, etc.[40]

Herein, a ratiometric fluorescent probe (SiNPs@AC-CA-Eu) was fabricated for rapid detection of DPA. The SiNPs as a fluorescence interior reference were uniformly loaded on the

https://doi.org/10.1021/acs.analchem.4c00443
Anal. Chem. 2024, 96, 6012−6020

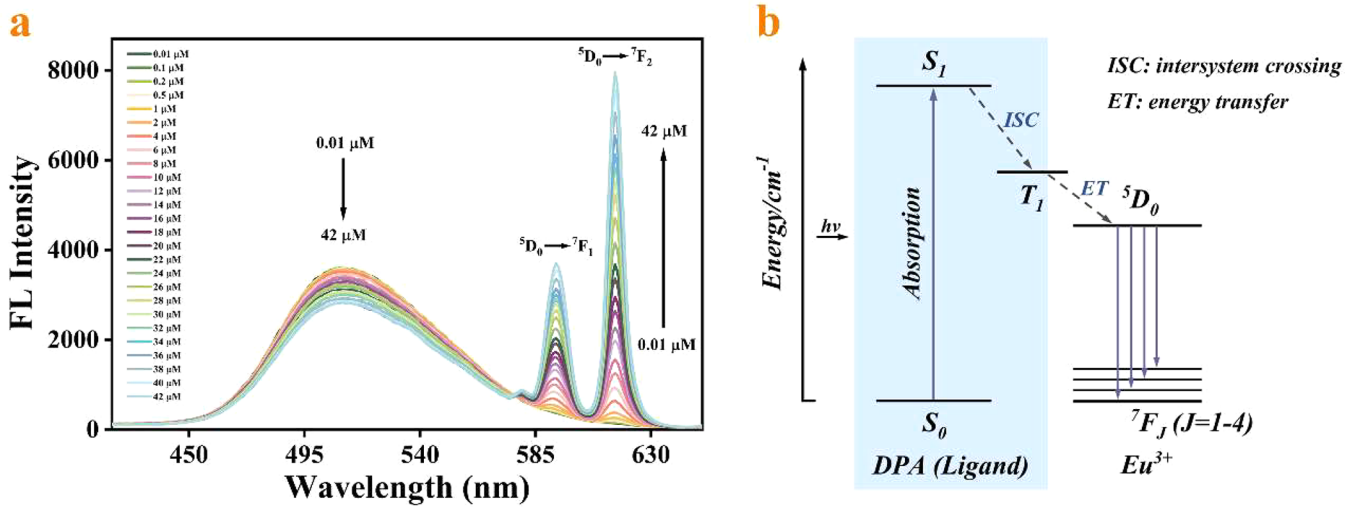

Figure 2. (a) Fluorescence spectra of the probe upon the addition of DPA at various concentrations. (b) Simplified schematic energy transfer between the analyte and the probe.

aminoclay and encapsulated into its layers, while europium ions as a specific recognition unit were grafted onto the surface of citrate-modified aminoclay via coordination interaction. The as-prepared hybrid nanoprobe comprises the merits of lanthanide ions together with the advantages of SiNPs, accomplishing the purpose of amplifying ratiometric response signals and achieving multicolor variations. Upon the addition of DPA, the bright green fluorescence of SiNPs gradually declined rather than remained at a fixed intensity, and the intrinsic red fluorescence of Eu(III) was sensitized to turn on based on the antenna effect. Not only examined for DPA determination, the proposed method was also utilized for detection of *Bacillus subtilis* spores (*B. subtilis* spores), which were commonly used as the harmless simulants for *B. anthracis* spores, as well as real environmental samples including lake water, tap water, and soil. Additionally, this ratiometric fluorescent strategy with profuse color evolution was conducive to realizing visual quantification of target analytes with assistance of color analysis APP on a smartphone, showing the potential of real-time on-site sensing application free from laboratory equipment or professionals.

EXPERIMENTAL SECTION

Synthesis of the Probe. The synthetic procedures of the probe were illustrated in Scheme 1, while detailed preparation routes were expounded in the Supporting Information sections S2.1−S2.3.

Fluorescence Determination of DPA in Standard Solutions and Simulant *B. subtilis* Spores. A 300 μL aliquot of borax buffer solution (0.1 M, pH 9.0), 100 μL of probe solution, and 100 μL of DPA solution at a certain concentration ranging from 0.01 to 42 μM were in sequence added into a 2 mL centrifuge tube. After shaking the prepared standard solutions thoroughly for 10 s at room temperature, fluorescence emission spectra of the system excited at 270 nm were measured in a 1 cm quartz cuvette. The intensity ratio of fluorescent emission at 511 and 616 nm (F_{616}/F_{511}) excited at 270 nm was calculated for quantitation of DPA.

For determination of *B. subtilis* spores, the spore stock suspension (10^9 CFU·mL^{-1}) was diluted to different concentrations and each sample was treated according to the literature[41] with slight modifications as follows: 295 μL of spore suspension was added into sterile tube, followed by 5 μL of dodecylamine solution (20 mM), then the tube was incubated in a water bath of 90 °C for 30 min to stimulate the germination of *B. subtilis* spores accompanied by the release of DPA from budding spores. After the mixture was cooled to room temperature, 100 μL of borax buffer solution and 100 μL of probe solution were mixed with this 300 μL of germinated spore suspension, and the following determination procedures were the same as described above.

Construction of Smartphone-Assisted RGB Analysis. Considering that the successive color change of the sensing system could be directly observed under UV irradiation, a smartphone-assisted RGB analysis was fabricated for visual quantitation, drawing on our previous experience.[42] Details of the visual quantitative determination by analyzing RGB values obtained from an APP installed on a smartphone were as follows. The reaction solutions of different analytes were all photographed under 254 nm irradiation with a UV lamp in the dark. Via a color recognition application called "color extract" on the smartphone, information on the colors in the images could be converted into corresponding RGB values for subsequent processing data. Ultimately, relation curves between the green/red value of the sensing system and the concentration of analytes could be gained.

RESULTS AND DISCUSSION

Morphology and Structure Characterization. The morphologies of the SiNPs and probe were clearly verified by transmission electron microscopy (TEM). As shown in Figure S1, SiNPs were dispersive spherical nanoparticles with an average diameter of 3.3 nm, and the high-resolution TEM image inset in Figure S1 displayed obvious lattice fringes. As for the probe, since aminoclay is an organic aminopropyl magnesium silicate material with special lamellar structure,[43] SiNPs were uniformly scattered in flake aminoclay after encapsulated in its layer as observed in Figure 1. As the europium complexes were also grafted on the surface of aminoclay, the EDS elemental mapping analysis proved the existence of C, N, O, Si, Mg, and Eu elements, suggesting the successful formation of the SiNPs@AC-CA-Eu probe. The ζ potentials of precursor SiNPs, intermediate, and the probe were measured as shown in Figure S2a, the results of which

https://doi.org/10.1021/acs.analchem.4c00443
Anal. Chem. 2024, 96, 6012−6020

demonstrated the synthesis of the probe once again. Structure of the probe was characterized by Fourier transform infrared (FT-IR), X-ray photoelectron spectroscopy (XPS), and X-ray diffraction (XRD) analyses and compared with those of precursor SiNPs, intermediate products (Figures S3, S4, S5, and S6). These detailed descriptions were listed in the Supporting Information section S3. Moreover, a photograph of the probe and illustration showing its proposed surface functionalized structure were also supported in Figure S7. Optical properties and stability of the probe (Figures S8 and S9) were elaborated in Supporting Information section S4, while optical characteristics of the precursor SiNPs were listed in Figure S10 for comparison.

Sensing Mechanism of the Fluorescent Assay. It is well-known that europium ions as lanthanide ions own intrinsic narrow line emission bands; however, trivalent europium ions alone in aqueous solution exhibited pretty low self-luminous efficiency under direct excitation of ultraviolet light as shown in Figure S11a, on account of the Laporte forbidden f−f transitions and the nonradiative transition from excited states of Eu^{3+} ions to vibrational relaxation of water molecules. Also proved by experiment, Eu^{3+} ions alone (1 mg/mL) did not have a detectable fluorescence lifetime. While Eu(III) in the fabricated sensing probe were grafted onto the surface of SiNPs@AC through chelating with auxiliary ligand citrate, the fluorescence lifetime of the probe at 616 nm corresponding to the characteristic emission band of Eu(III) was measured as 2.957 ns (Figure S12a); meanwhile, the fluorescence lifetime of the probe at 511 nm corresponding to the emission peak of SiNPs was 3.182 ns, marginally shorter than that of the pure SiNPs as 3.298 ns, under 280 nm excitation (the excitation wavelength of the laser available to select that was the most proximate to the experimental excitation wavelength of 270 nm). Inferred from these phenomena, a certain degree of energy transfer may exist from SiNPs to Eu(III) in the probe.

As revealed in Figure 2, the intensity of the characteristic fluorescence emission from Eu(III) in the probe continually increased with the unremittingly increased concentration of DPA, hence the need for an inquiry of fluorescence lifetime. It was detailed in Figure S12b that upon the addition of analyte DPA, the fluorescence lifetime of the probe at 511 nm scarcely showed much change. In contrast, the fluorescence lifetime of the probe at 616 nm displayed tremendous fluctuations (Figure S12c,d). Specifically, the fluorescence lifetime of the probe at 616 nm was significantly enhanced as the concentration of the added DPA increased, while that at 511 nm was faintly reduced a little bit. Moreover, DPA possessed an obvious absorption band at 273 nm in the UV−vis absorption spectrum (Figure S11b), which was close to the excitation wavelength of the used laser. According to the above, the sensing mechanism can be summarized as follows: the analyte DPA as ligand coordinated with europium ions of the probe, then transferred the absorbed energy to the europium ions, leading to characteristic fluorescence emission of the sensitized europium ions, the process of which is called "antenna effect" or sensitization, and DPA acted as "antenna" that could sensitize the europium ions. It could also be found in Figure S11a that the characteristic emission of europium ions in the Eu^{3+}-DPA system was lower than that in probe-DPA system, probably for the reason that after coordinated with DPA but still not saturated, the europium ions in Eu(III)-DPA system thereby chelated with water molecules resulting in such energy loss.[26] The europium ions in the probe-DPA system not only chelated with DPA but also coordinated with the carboxyl groups from the CA-modified probe, thus protected from water and fully boosting the fluorescence enhancement. Additionally, the ζ potentials of the probe and mixtures of the probe with DPA at different concentrations were explored. It turned out from Figure S2b that the ζ potentials of the probe with different concentrations of DPA were almost unchanged, indicating the response of the probe toward DPA was independent of surface charge. The FT-IR spectrum of the probe was also compared with that of the probe mixed with DPA in Figure S13b, and it appeared that the bands at 1609 cm^{-1}, 1218 cm^{-1}, and 1031 cm^{-1} had blue-shift, further verifying the coordination interaction between the probe and DPA.

A schematic representation of the energy transfer process from DPA to the probe was illustrated in Figure 2b. Analyte DPA, as the ligand of Eu(III), absorbed energy and underwent electron transition from ground state S_0 to excited singlet state S_1, then transferred to excited triplet state T_1 with lower energy through intersystem crossing. On the one hand, since the excited state ($^5D_0$) energy level of Eu(III) was even lower than the lowest triplet excitation level of DPA, an effective energy transfer was able to occur from DPA to Eu(III). On the other hand, DPA possessed a greater coordination ability to chelate with Eu(III) and substituted the coordinated water molecules, lessening the nonradiative energy loss arising from the high-frequency vibration of O−H, thus restoring the sensitization toward luminescence features of Eu(III). Based on these two points, europium ions smoothly obtained the energy efficiently transferring from triplet state DPA and then transited to the excited state $^5D_0$; the characteristic red fluorescence was emitted once the electrons of Eu(III) returned from excited state to ground state.

Fluorometric Performance of DPA and *B. subtilis* Spore Determination. In the absence of DPA, the probe only exhibited an emission peak at 511 nm with green fluorescence under the excitation of 270 nm. The characteristic emission of Eu(III) was not turned on yet, attributable to the unsaturation coordination of europium ions and the non-radiation quenching effect of the coordinated water molecules. Upon the addition of analyte DPA, the transitions of Eu(III) from the excited state $^5D_0$ to the ground state of ^7F_J (J = 1,2,3,4) caused the peaks at 593 nm, 616 nm, 650 nm, and 695 nm in sequence, among which the emission peaks belonging to $^5D_0 \rightarrow {}^7F_3$ and $^5D_0 \rightarrow {}^7F_4$ (located at 650 and 695 nm) were so faint that they could be certainly negligible, whereas the prominent transition of $^5D_0 \rightarrow {}^7F_2$ (located at 616 nm) was the most hypersensitive and thus assigned as the sensing signal (Figure 2a).

It could be observed from Figure S15a that with an increasing concentration of DPA, the red emission at 593 and 616 nm originating from Eu(III) constantly strengthened, puny peaks at 650 and 695 nm remained inappreciable whether the concentration of DPA was high or low, while the green fluorescence stemming from the SiNPs gradually declined to some extent that could serve as an internal reference signal to construct a ratiometric fluorescent sensing system. Under the optimal conditions (Figure S14), the intensity ratio of fluorescent emission peaks at 616 and 511 nm (F_{616}/F_{511}) of the probe linearly correlated with the concentration of DPA at a range of 0.05−10.00 μM (Figure S15b), and the limit of detection (LOD) was calculated as 0.02

https://doi.org/10.1021/acs.analchem.4c00443
Anal. Chem. 2024, 96, 6012−6020

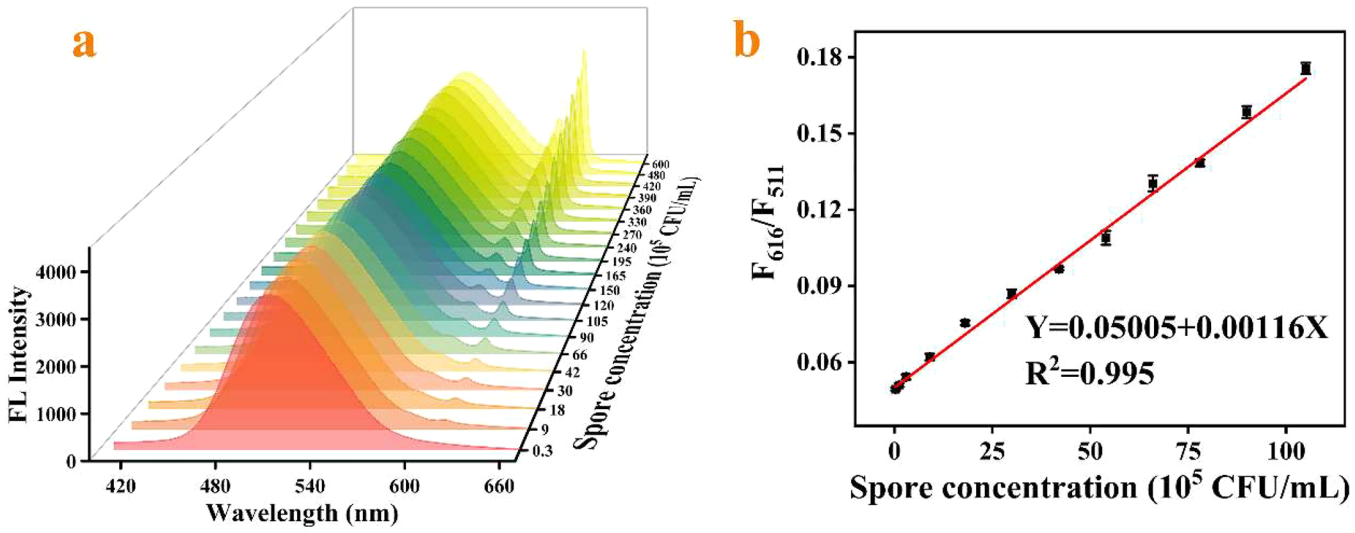

Figure 3. (a) 3D fluorescent spectra plot of the probe response to different concentrations of *B. subtilis* spores. (b) Linear plot of F_{616}/F_{511} versus *B. subtilis* spore concentration from 0.3 × 10^5 to 105.0 × 10^5 CFU/mL.

μM based on $3\sigma/k$ (σ was the standard deviation of 11 blank responses, k was the slope of linear calibration curve), which was much lower than an infectious dosage of the spores (60 μM required). Moreover, the CIE chromaticity diagram showing the fluorescence changes of the system under different DPA concentrations was demonstrated as shown in Figure S16. The fluorescent color coordinates fit an excellent linear relationship as a function of DPA concentration, which is y = 0.6487 − 0.451x (R^2 = 0.999), and the chromaticity coordinates of the sensing system with DPA concentration varying from 0.01 to 42.00 μM were enumerated in Table S1. Apparently, the related concentration of DPA could be evaluated from the color varying tendency along the direction of the line inset in Figure S16. In addition, selectivity and anti-interference capacity of the probe were evaluated and are expounded in the Supporting Information section S6. Considering the outstanding specificity and sensitivity of the probe for the DPA determination (Figure S18), it was inferred that this sensing system could also be suitable for the detection of pathogenic bacteria spores, such as *B. anthracis* spores. Thinking through the high risk of aggressiveness and infectivity of *B. anthracis* spores, the noninfectious *B. subtilis* spores were finally employed as model spores. Similarly, the probe also could be sensitized for red-emission fluorescence by suspension of stimulated *B. subtilis* spores rather than the ungerminated one (Figure S11c), the emission ratio F_{616}/F_{511} progressively increased with the increasing concentration of *B. subtilis* spores as displayed in Figure 3a, and a good linear relationship at range of 0.3 × 10^5 to 105.0 × 10^5 CFU/mL (R^2 = 0.995) was achieved with the LOD of 0.17 × 10^5 CFU/mL (Figure 3b). Besides, the overall fluorescence response curve of either DPA or *B. subtilis* spore was provided in Figure S19.

Smartphone-Assisted RGB Analysis. Since the system exhibited an obviously discriminative color variation with an increasing concentration of the analyte, it enabled the possibility of realizing an accurate visual sensing by analyzing RGB values of the fluorescent color corresponding to the test sample. The process was illustrated in Figure 4a, and the images in Figure 4b and Figure 4c both showed the color changes of DPA sensing system except that the concentration of the probe in Figure 4c was higher than that in Figure 4b. And the image in Figure 4d displayed the multicolor variation of the *B. subtilis* spore sensing system. It could be observed that the system color steadily changed from jade green to light green, yellowish green, lemon yellow, carrot orange, red as the concentration of DPA or *B. subtilis* spores gradually increased. Since the suspension of *B. subtilis* spore at large concentration is a slightly cloudy and whitish liquid, solutions in tubes along the right side seemed a little pallid in Figure 4d. In the DPA sensing system of Figure 4b, the green/red value of the image displayed good linear relationships toward DPA concentration, respectively corresponding to an interval of 0.5−30.0 μM with regression equation G/R = 2.1262 − 0.0294[DPA] (R^2 = 0.999) and another interval of 60−150 μM with regression equation G/R = 1.1484 − 0.00402[DPA] (R^2 = 0.986). While in the *B. subtilis* spore sensing system of Figure 4d, regression equations could be fitted as G/R = 2.4046 − 0.00178[*B. subtilis* spores] (R^2 = 0.998) within the scope of 3 × 10^5 to 570 × 10^5 CFU/mL and G/R = 1.5286 − 0.000412[*B. subtilis* spores] (R^2 = 0.995) within the scope of 810 × 10^5 to 2010 × 10^5 CFU/mL. Figure 4c illustrated the color change of the sensing system with the concentration of DPA rising from 0.5 μM to 1.0 mM when the concentration of the probe increased to 4 times the original one; the fluorescent colors also seemed more vivid and bright in Figure 4c than those in Figure 4b. Similarly, the G/R value correlated linearly with DPA concentration elevated from 250 to 600 μM (R^2 = 0.991), thus inferring that if an appropriate concentration of probe was selected and applied in the sensing system, it is very likely to achieve the visual quantitative detection of analytes in various concentration ranges, widening the extent of application.

Application in Real Environmental Samples. Aiming to investigate the practicability of this sensing tactic, several real environmental samples including lake water, tap water, and soil were utilized, and the results were expounded in Table 1. All the measured data listed in the tabulation were average values of three parallel measurements ± standard deviation. It can be seen that no presence of such spores was found in any of the original real samples. By spiking a series of different concentrations of *B. subtilis* spore suspension into diverse real samples, the accuracy and utility of the proposed method were confirmed and satisfactory recoveries between 98.83%

https://doi.org/10.1021/acs.analchem.4c00443
Anal. Chem. 2024, 96, 6012−6020

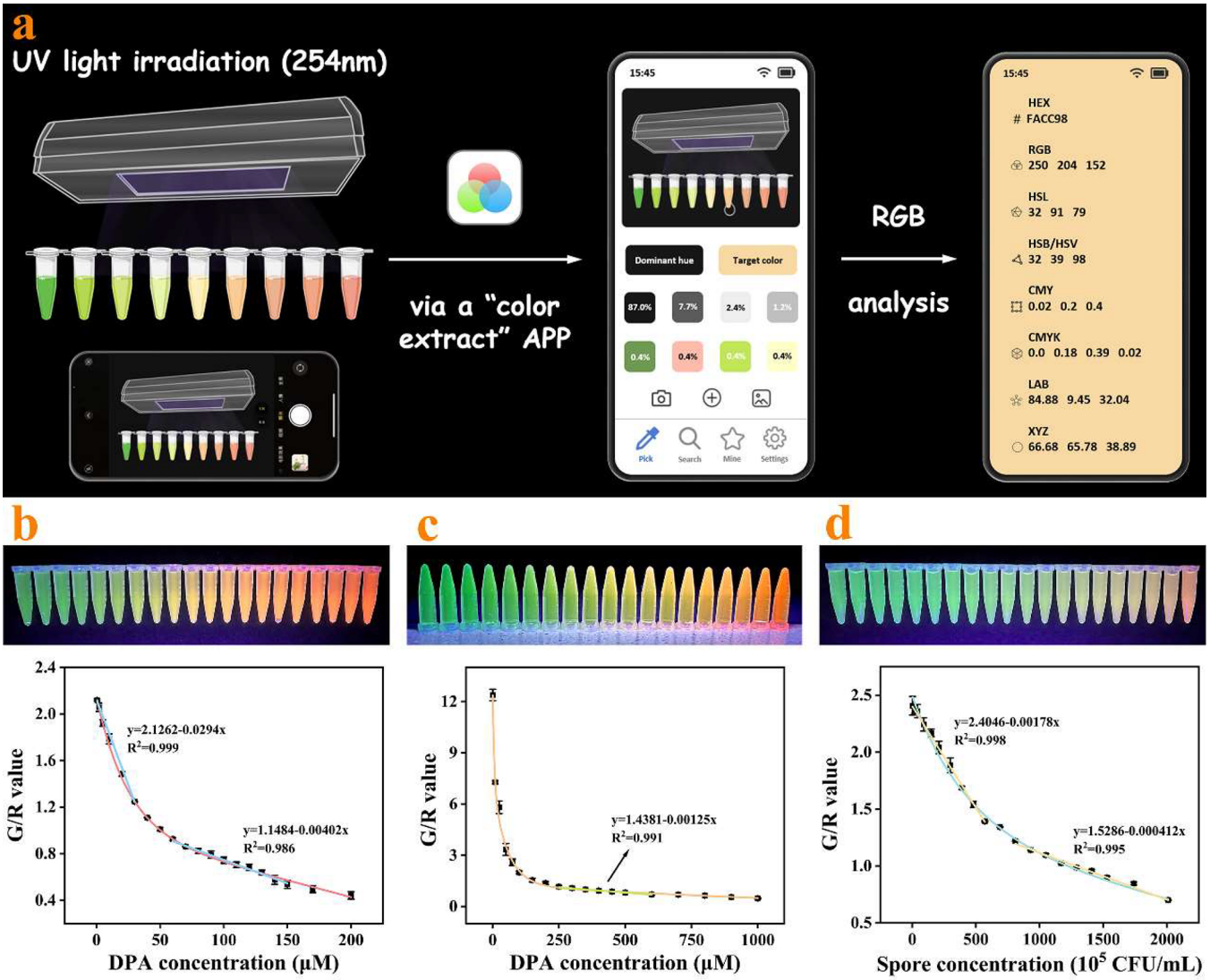

Figure 4. (a) RGB analysis of the smartphone-assisted mode via a color recognition APP. The rest of the images below are photographs of the sensing systems and their corresponding RGB analysis curves. (b) Change of the green/red value ratio of the image versus DPA concentration from 0.5 to 200.0 μM with the concentration of the probe as 0.5 mg/mL. The concentrations of DPA in the 500 μL centrifugal tubes from left to right in the upper image were 0.5, 2, 5, 10, 20, 30, 40, 50, 60, 70, 80, 90, 100, 110, 120, 130, 140, 150, 170, and 200 μM. (c) Change of the green/red value ratio of the image versus DPA concentration from 0.5 μM to 1 mM with the concentration of the probe as 2.0 mg/mL. The concentrations of DPA in tubes from left to right in the upper image were 0.5, 10, 25, 50, 75, 100, 150, 200, 250, 300, 350, 400, 450, 500, 600, 700,800, 900, 1000 μM. (d) Change of the green/red value ratio of the image versus *B. subtilis* spore concentration from 3×10^5 to 2010×10^5 CFU/mL with the concentration of the probe as 0.5 mg/mL. The concentrations of *B. subtilis* spores in tubes from left to right in the upper image were 3, 18, 42, 90, 15, 210, 300, 390, 480, 570, 690, 810, 930, 1050, 1170, 1290, 1410, 1530, 1740, 2010×10^5 CFU/mL in sequence.

and 107.64% were secured with each of the measured outcomes having a low relative standard deviation (RSD, n = 3) less than 7.5%. In conclusion, the established sensing strategy possessed such splendid feasibility and applicability that it was competent for detecting the pathogenic bacteria spores in an actual complex environment. Comparisons of the analytical performance between this approach and other published methods for sensing DPA and *B. subtilis* spores were scheduled in Tables S2 and S3, respectively. Overall, the present approach demonstrated such superiorities of agile responsiveness, high sensitivity, and excellent specificity over most of others, further showing a great potential for rapid on-site assessment.

CONCLUSION

In this study, we successfully established a europium(III)-functionalized SiNPs-containing hybrid nanoprobe for rapid ratiometric fluorescent sensing of pathogenic bacteria spore biomarker DPA. Europium ions emitting red fluorescence were set as an identification response unit, while SiNPs showing green fluorescence acted as an internal reference standard. The proposed sensing method was also favorably applied in the determination of *B. subtilis* spores and simulants for *B. anthracis* spores and examination of real environmental samples. Considering the sensing system presenting multicolor variations in response to different concentrations of the analyte, sensitive visual detection was achieved via analysis of RGB values of a system color aided by the color recognition APP on a smartphone, providing an effective pathway for real-

https://doi.org/10.1021/acs.analchem.4c00443
Anal. Chem. 2024, 96, 6012−6020

Table 1. Analysis Results of *Bacillus subtilis* Spores in Environmental Samples by the Proposed Method[a]

sample	found (×10^5 CFU/mL)	spiked (×10^5 CFU/mL)	total found (×10^5 CFU/mL)	recovery (%)	RSD (%)
Qing Lake water	NF	0.5	0.50 ± 0.03	100.69	5.43
		10	10.41 ± 0.14	104.14	1.32
		20	19.90 ± 0.18	99.51	0.90
		40	40.57 ± 1.55	101.43	3.83
Yan Lake water	NF	1.1	1.14 ± 0.08	103.60	7.37
		16	16.23 ± 0.24	101.46	1.50
		32	31.80 ± 0.40	99.37	1.27
		64	63.64 ± 1.06	99.44	1.66
tap water	NF	1.7	1.83 ± 0.09	107.64	4.67
		27	27.69 ± 0.49	102.56	1.77
		54	54.66 ± 1.38	101.23	2.53
		108	108.61 ± 1.97	100.56	1.81
soil	NF	2.3	2.37 ± 0.13	102.83	5.41
		35	35.60 ± 0.94	101.72	2.65
		70	69.18 ± 0.85	98.83	1.23
		140	142.19 ± 1.82	101.57	1.28

[a]NF: not found.

time on-site applicability. Based on the above performances, we envision that the simple strategy with excellent selectivity and outstanding anti-interference capability would hold great application prospects in food safety, environmental security, health supervision, and clinical diagnosis fields.

■ ASSOCIATED CONTENT

Supporting Information

The Supporting Information is available free of charge at https://pubs.acs.org/doi/10.1021/acs.analchem.4c00443.

Additional experimental details, including reagents and instruments; experimental procedures; characterization of the probe and SiNPs; optimization of experimental conditions; selectivity and anti-interference capacity of the strategy; supplementary figures and tables (PDF)

■ AUTHOR INFORMATION

Corresponding Authors

Pinyi Ma − *Jilin Province Research Center for Engineering and Technology of Spectral Analytical Instruments, College of Chemistry, Jilin University, Changchun 130012, China;* orcid.org/0000-0002-3230-4928; Email: mapinyi@jlu.edu.cn

Qiong Wu − *Key Laboratory of Pathobiology, Ministry of Education, Nanomedicine and Translational Research Center, China-Japan Union Hospital of Jilin University, Changchun 130030, China*; Email: qiong_wu@jlu.edu.cn

Daqian Song − *Jilin Province Research Center for Engineering and Technology of Spectral Analytical Instruments, College of Chemistry, Jilin University, Changchun 130012, China;* orcid.org/0000-0002-4866-1292; Email: songdq@jlu.edu.cn

Authors

Xiwen Ye − *Jilin Province Research Center for Engineering and Technology of Spectral Analytical Instruments, College of Chemistry, Jilin University, Changchun 130012, China*

Jingkang Li − *Jilin Province Research Center for Engineering and Technology of Spectral Analytical Instruments, College of Chemistry, Jilin University, Changchun 130012, China*

Dejiang Gao − *Jilin Province Research Center for Engineering and Technology of Spectral Analytical Instruments, College of Chemistry, Jilin University, Changchun 130012, China*

Complete contact information is available at: https://pubs.acs.org/10.1021/acs.analchem.4c00443

Notes

The authors declare no competing financial interest.

■ ACKNOWLEDGMENTS

This work was supported by the National Natural Science Foundation of China (Grants 22074052 and 22004046).

■ REFERENCES

(1) Setlow, B.; Cowan, A. E.; Setlow, P. *J. Appl. Microbiol.* **2003**, *95*, 637−648.

(2) Aronson, A. I.; Fitz-James, P. *Bacteriological reviews* **1976**, *40*, 360−402.

(3) Albert, H.; Davies, D. J.; Woodson, L. P.; Soper, C. J. *J. Appl. Microbiol.* **1998**, *85*, 865−874.

(4) Bhardwaj, N.; Bhardwaj, S.; Mehta, J.; Kim, K.-H.; Deep, A. *Biosens. Bioelectron.* **2016**, *86*, 799−804.

(5) Cable, M. L.; Kirby, J. P.; Sorasaenee, K.; Gray, H. B.; Ponce, A. *J. Am. Chem. Soc.* **2007**, *129*, 1474−1475.

(6) Li, Q.; Sun, K.; Chang, K.; Yu, J.; Chiu, D. T.; Wu, C.; Qin, W. *Anal. Chem.* **2013**, *85*, 9087−9091.

(7) Ai, K.; Zhang, B.; Lu, L. *Angew. Chem., Int. Ed.* **2009**, *48*, 304−308.

(8) Yung, P. T.; Shafaat, H. S.; Connon, S. A.; Ponce, A. *FEMS Microbiol. Ecol.* **2007**, *59*, 300−306.

(9) Barakat, L. A.; Quentzel, H. L.; Jernigan, J. A.; Kirschke, D. L.; Griffith, K.; Spear, S. M.; Kelley, K.; Barden, D.; Mayo, D.; Stephens, D. S.; Popovic, T.; Marston, C.; Zaki, S. R.; Guarner, J.; Shieh, W.-J.; Carver Ii, H. W.; Meyer, R. F.; Swerdlow, D. L.; Mast, E. E.; Hadler, J. L.; for the Anthrax Bioterrorism Investigation, T.. *JAMA* **2002**, *287*, 863−868.

(10) Borio, L.; Frank, D.; Mani, V.; Chiriboga, C.; Pollanen, M.; Ripple, M.; Ali, S.; DiAngelo, C.; Lee, J.; Arden, J.; Titus, J.; Fowler, D.; O'Toole, T.; Masur, H.; Bartlett, J.; Inglesby, T. *JAMA* **2001**, *286*, 2554−2559.

(11) Mock, M.; Fouet, A. *Annu. Rev. Microbiol.* **2001**, *55*, 647−671.

(12) Pile, J. C.; Malone, J. D.; Eitzen, E. M.; Friedlander, A. M. *Arch. Int. Med.* **1998**, *158*, 429−434.

(13) Dixon, T. C.; Meselson, M.; Guillemin, J.; Hanna, P. C. *New Engl. J. Med.* **1999**, *341*, 815−826.
(14) Zhang, X.; Young, M. A.; Lyandres, O.; Van Duyne, R. P. *J. Am. Chem. Soc.* **2005**, *127*, 4484−4489.
(15) Bhardwaj, N.; Bhardwaj, S.; Mehta, J.; Kim, K.-H.; Deep, A. *Biosens. Bioelectron.* **2016**, *86*, 799−804.
(16) Holty, J. E. C.; Bravata, D. M.; Liu, H.; Olshen, R. A.; McDonald, K. M.; Owens, D. K. *Ann. Intern. Med.* **2006**, *144*, 270−280.
(17) Black, S. H.; Macdonald, R. E.; Hashimoto, T.; Gerhardt, P. *Nature* **1960**, *185*, 782−783.
(18) Das, R.; Goel, A. K.; Sharma, M. K.; Upadhyay, S. *Biosens. Bioelectron.* **2015**, *74*, 939−946.
(19) Tang, S.; Moayeri, M.; Chen, Z.; Harma, H.; Zhao, J.; Hu, H.; Purcell, R. H.; Leppla, S. H.; Hewlett, I. K. *Clin. Vaccine Immunol.* **2009**, *16*, 408−413.
(20) Fasanella, A.; Losito, S.; Adone, R.; Ciuchini, F.; Trotta, T.; Altamura, S. A.; Chiocco, D.; Ippolito, G. *J. Clin. Microbiol.* **2003**, *41*, 896−899.
(21) Walt, D. R.; Franz, D. R. *Anal. Chem.* **2000**, *72*, 738A−746A.
(22) Gao, N.; Zhang, Y.; Huang, P.; Xiang, Z.; Wu, F.-Y.; Mao, L. *Anal. Chem.* **2018**, *90*, 7004−7011.
(23) Bailey, G. F.; Karp, S.; Sacks, L. E. *J. Bacteriol.* **1965**, *89*, 984−987.
(24) Powell, J. F. *Biochem. J.* **1953**, *54*, 210−211.
(25) Huang, S.-s.; Chen, D.; Pelczar, P. L.; Vepachedu, V. R.; Setlow, P.; Li, Y.-q. *J. Bacteriol.* **2007**, *189*, 4681−4687.
(26) Luan, K.; Meng, R.; Shan, C.; Cao, J.; Jia, J.; Liu, W.; Tang, Y. *Anal. Chem.* **2018**, *90*, 3600−3607.
(27) He, K.; Li, Z.; Wang, L.; Fu, Y.; Quan, H.; Li, Y.; Wang, X.; Gunasekaran, S.; Xu, X. *ACS Appl. Mater. Interfaces* **2019**, *11*, 26250−26260.
(28) Tsukube, H.; Shinoda, S. *Chem. Rev.* **2002**, *102*, 2389−2404.
(29) Hanaoka, K.; Kikuchi, K.; Kobayashi, S.; Nagano, T. *J. Am. Chem. Soc.* **2007**, *129*, 13502−13509.
(30) Oh, W.-K.; Jeong, Y. S.; Song, J.; Jang, J. *Biosens. Bioelectron.* **2011**, *29*, 172−177.
(31) Xu, H.; Rao, X.; Gao, J.; Yu, J.; Wang, Z.; Dou, Z.; Cui, Y.; Yang, Y.; Chen, B.; Qian, G. *Chem. Commun.* **2012**, *48*, 7377−7379.
(32) Tan, H.; Ma, C.; Chen, L.; Xu, F.; Chen, S.; Wang, L. *Sensor. Actuat. B-Chem.* **2014**, *190*, 621−626.
(33) Wang, Y.; Li, Y.; Qi, W.; Song, Y. *Chem. Commun.* **2015**, *51*, 11022−11025.
(34) Xu, J.; Shen, X.; Jia, L.; Zhang, M.; Zhou, T.; Wei, Y. *Biosens. Bioelectron.* **2017**, *87*, 991−997.
(35) Bu, X.; Fu, Y.; Jiang, X.; Jin, H.; Gui, R. *Microchim. Acta* **2020**, *187*, 154.
(36) Chen, Y.; Zhu, C.; Yang, Z.; Chen, J.; He, Y.; Jiao, Y.; He, W.; Qiu, L.; Cen, J.; Guo, Z. *Angew. Chem., Int. Ed.* **2013**, *52*, 1688−1691.
(37) McVey, B. F. P.; Tilley, R. D. *Acc. Chem. Res.* **2014**, *47*, 3045−3051.
(38) Li, D.; Li, N.; Zhao, L.; Xu, S.; Sun, Y.; Ma, P.; Song, D.; Wang, X. *ACS Appl. Nano Mater.* **2020**, *3*, 11600−11607.
(39) Datta, K. K. R.; Achari, A.; Eswaramoorthy, M. *J. Mater. Chem. A* **2013**, *1*, 6707−6718.
(40) Li, Q.-F.; Liu, Z.; Jin, L.; Yang, P.; Wang, Z. *RSC Adv.* **2017**, *7*, 44614−44618.
(41) Li, X.; Luo, J.; Deng, L.; Ma, F.; Yang, M. *Anal. Chem.* **2020**, *92*, 7114−7122.
(42) Ye, X.; Gao, D.; Mu, X.; Wu, Q.; Ma, P.; Song, D. *Anal. Chem.* **2023**, *95*, 4653−4661.
(43) Bi, N.; Xi, Y. H.; Hu, M. H.; Xu, J.; Gou, J.; Li, Y. X.; Zhang, L. N.; Jia, L. *Microchim. Acta* **2022**, *189*, 462.

https://doi.org/10.1021/acs.analchem.4c00443
Anal. Chem. 2024, 96, 6012−6020